Trends of total reaction cross sections for heavy ion collisions in the intermediate energy range

S. Kox,[a] A. Gamp,*[a],[b] C. Perrin,[a] J. Arvieux,†[a] R. Bertholet,[c] J. F. Bruandet,[a] M. Buenerd,[a] R. Cherkaoui,‡[a] A. J. Cole,[a] Y. El-Masri,[a],[d] N. Longequeue,[a] J. Menet,[a] F. Merchez,[a] and J. B. Viano[a]

[a]*Institut des Sciences Nucléaires de Grenoble, 38026 Grenoble, Cédex, France*

[b]*Hahn Meitner Institut für Kernforschung, Berlin, Federal Republic of Germany*

[c]*Département de Recherche Fondamentale, Centre d'Etudes Nucléaires, 38026 Grenoble, Cédex, France*

[d]*Institut de Physique Nucléaire, Université de Louvain, Louvain-la-Neuve, Belgium*

(Received 10 October 1986)

Direct measurements of total reaction cross sections (σ_R) have been performed in the energy range of 10—300 MeV/nucleon for heavy ion collisions. A decrease of σ_R with increasing energy was observed for a wide range of masses of the colliding systems. The data suggest that σ_R reaches a minimum located around 300 MeV/nucleon independently of the projectile target combination. A dependence of σ_R on mass asymmetry of the system is also demonstrated. Trends of σ_R in this energy range are well reproduced by the predictions of a simple microscopic model based on individual nucleon-nucleon collisions. Our data have been employed in this framework to derive a new semi-empirical parametrization of σ_R. Most of the experimental results in the intermediate and high energy range have been reproduced by this parametrization using a single energy-dependent parameter.

I. INTRODUCTION

The total reaction cross section (σ_R) has been extensively studied both theoretically[1–19] and experimentally[20–40] for more than 40 years. A considerable amount of work has also been devoted to the determination of a general parametrization[41–47] of this fundamental observable characterizing nuclear collisions. This interest was revitalized by DeVries *et al.*,[12] who addressed the description of complex nuclear reactions in the intermediate energy range in terms of individual nucleon-nucleon (N-N) collisions. They succeeded in reproducing (even at energies as low as 10—30 MeV/nucleon) the different trends of the σ_R data for N-nucleus systems using a simple microscopic model. This agreement simply linked the decrease of σ_R with that of the individual N-N total cross section (σ_T^{NN}), and demonstrated the important role of these collisions at intermediate energies. A lack of experimental data (in Ref. 12) did not permit a test of the reliability of this approach to heavy ion collisions.

With the recent availability of heavy ions beams in the intermediate energy range (from the accelerators SARA, GANIL, SATURNE, and S.C. CERN), data have been obtained by various experimental techniques.[32–40] In this article we report a compilation of our measurements for heavy ion reactions between 10 and 300 MeV/nucleon and over a wide mass range.

In Sec. II we present the basis of our experimental method and describe the setup for these experiments. Section III is devoted to the data handling and its reliability. In Sec. IV the data are compared to predictions of models originally developed for lower and higher projectile energies and extrapolated to this energy range. The physical interpretation of the general trends of our data is also discussed in the framework of a simple microscopic model. In the last section we give details of a new parametrization that we proposed earlier for the description of σ_R in the intermediate and high energy range. We conclude with a summary and comments.

II. EXPERIMENTAL DETAILS

A. Principles of the method

Our goal was to obtain total reaction cross sections by a direct measurement technique. The values of σ_R thus extracted are essentially model independent, in contrast to those determined from analyses of elastic scattering data. Systematic measurements of σ_R have been made for many reactions with very efficient use of beam time. One should remark that direct measurement techniques have been seldom employed despite their advantages.[25,32,34,40] This is mainly due to their inherent experimental difficulties.

Our technique was based on the so-called beam attenuation (or transmission) method,[48] which has been previously used for the direct measurement of σ_R in proton-nucleus collisions.[22] In this technique one simply counts the number of beam particles incident on the target (N_{inc}), and the corresponding number of outgoing particles which have not undergone a reaction in the target (N_{el}). This latter number includes the particles elastically scattered and the residual beam particles (which are not distinguished in this experimental approach). The difference between these two numbers (N_{inc} and N_{el}) represents the number of reactions (N_{reac}) which occurred in the target for N_{inc} incident particles. If e is the target thickness, A its atomic mass, and $\mathcal{N}$ is Avogadro's number, then the value of σ_R can be expressed as

 ©1987 The American Physical Society

$$\sigma_R = \frac{(N_{\text{inc}} - N_{\text{el}})}{N_{\text{inc}}} \frac{A}{e\mathcal{N}} . \quad (1)$$

In this method, N_{inc} and N_{el} are statistically correlated as each nuclear event is observed individually. The corresponding statistical uncertainties associated with the measured value are thus calculated using the difference between these two numbers $[(N_{\text{inc}} - N_{\text{el}})^{1/2}]$.

B. The experimental setup

A schematic view of our experimental setup is shown in Fig. 1. It includes 21 counters, each composed of a fast plastic scintillator optically coupled to a photomultiplier by a light guide. This detector gives a high detection efficiency (assumed to 100%) for charged particles and allows high counting rates, which are especially desirable for detectors placed near or in the beam. The phototubes (RTC XP2020) were chosen for their good timing performance and the light collection was optimized by painting the light guides with a white reflector (NE 560).

1. The detectors placed upstream of the target

These two counters were used to determine the number of incident particles on the target. Counter 1 was a thin plastic scintillator placed on the beam axis and used to count incident particles. Its timing signal provided the start for a time of flight (TOF) measurement. The analog signal of this counter was also used to reject pileups that occurred for two or more incident particles. To be counted as a valid event, the beam particle had to produce an analog signal in a narrow pulse-height window corresponding to its energy loss in this counter. This window also permitted the rejection of any beam contamination. Counter 1 was also used to limit the beam intensity to less than 3×10^4 particles/s.

Counter 2 was an active collimator made from a thick plastic scintillator and was used to limit the size of the beam spot on the target. The entire setup was designed such that with no target the beam particles passing through counter 1 and through the hole of counter 2 were all detected in the central counter 3 downstream of the target. This collimator was also used to reject the forward scattered reaction residues produced by the beam in counter 1.

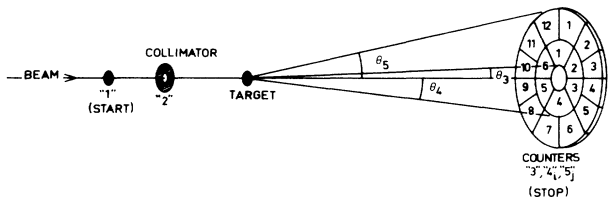

FIG. 1. Schematic drawing of the experimental setup. The beam on the target is defined by scintillators 1 and 2. The concentric rings around the central counter 3 in the "wheel" are labeled 4 and 5. The details of the various counters are described in the text.

2. The counters positioned downstream of the target

A set of 19 detectors was used to detect, identify, and count the residual beam and the elastically scattered projectiles emerging from the target. These counters were mounted in a "wheel" as schematized in Fig. 1 (cylindrically symmetric around the beam axis). The central counter 3 was surrounded by an inner ring of six counters ($4i$) and an outer one of 12 counters ($5j$). The cone subtended by the full detector setup exceeded (by 2—3 times) the grazing angle of each system studied. The distance between counters 1 and 3 was adjusted in order to fulfill this condition. Special care was taken to eliminate inefficient detection regions (dead spaces) in the vicinity of 0°. For this reason, a small overlap was provided between the scintillation material of the central counter 3 and the surrounding ones. The counters in rings $4i$ and $5j$ were mechanically attached to the aluminum skeleton of the "wheel" by appropriate supports which slightly overlapped the scintillator material. These supports were designed to preserve the cylindrical geometry of the active part of the detectors around the beam axis. An additional dead area was present between the two rings of counters $4i$ and $5j$. As the aluminum skeleton and the detector supports were accurately machined, the dead areas were accurately known.

The principle of our experimental approach requires discrimination between elastically scattered particles and reaction products emerging from the target. This discrimination has been achieved by detecting the light output induced by the charged particles in the scintillator in coincidence with their corresponding TOF. In fact, the organic scintillators[49,50] permit the identification of Z as shown in Fig. 2 for two typical runs. If a particle lost all its energy in the detectors, no such Z discrimination was possible. The scintillators thicknesses were thus chosen such that the elastically scattered particles would be stopped in the light guide. Timing signals from the counters downstream of the target were used as the TOF stop signals, the start having been generated by counter 1. In general, good Z identification was achieved for beam particles up to $Z=10$ with a light signal resolution around 7% and a time resolution of $\approx$500 ps (Fig. 2).

C. Electronics and data acquisition

In this subsection we restrict ourselves to the description of the most important and original aspects of the electronics. The number of beam particles incident on the target was defined by an anticoincidence between counter 1 and the active collimator 2 (with the conditions described above on the analog signal of counter 1). An additional electronic condition allowed the rejection of any pair of incident beam signals closer in time than 100—200 ns. A valid event was required to occur outside of the dead time (DT) period associated with the analysis of the preceding event. A special electronic device was used to control the data recording by taking into account both the counter and the computer dead times. Finally, the number of valid incident beam particles which fulfilled all the conditions described, was recorded. This number is given by the following function:

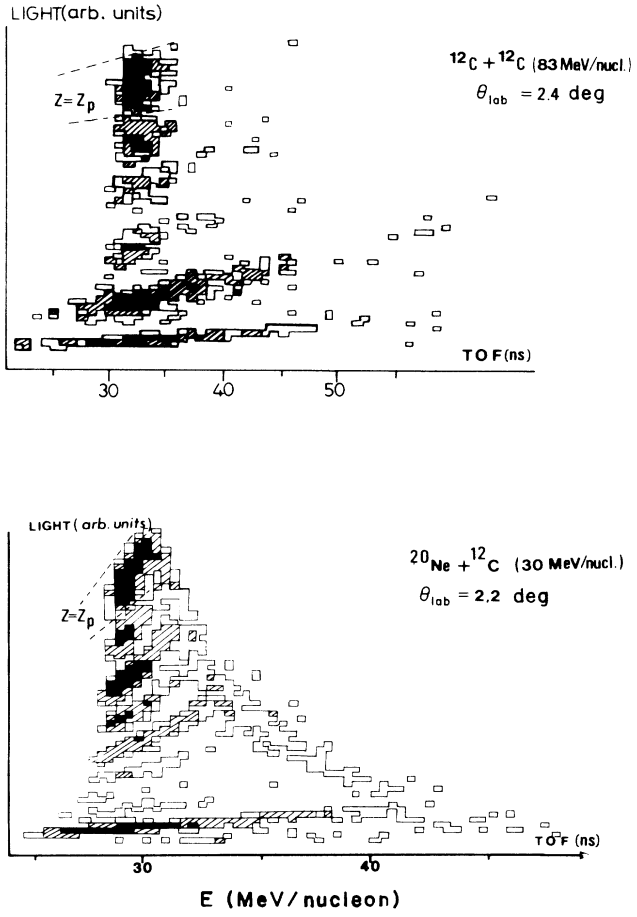

FIG. 2. Typical output from our counters at incident energies of 83 and 30 MeV/nucleon. The Z identification visible on the left-hand side of the figures is lost as ions are stopped in the scintillators.

$$F = 1 \times \bar{2} \times \overline{S_{DT}} \tag{2}$$

where S_{DT} is the dead time signal and the overbars denote anticoincidence. The value of F is strictly equal to N_{inc} needed for the derivation of σ_R [see Eq. (1)].

Dead time control was of crucial importance as the measured quantity $(N_{inc}-N_{el})/N_{inc}$ is very small ($\approx 10^{-3}$). The total dead time correction was applied to both the incident beam particle number (N_{inc}) and to the residual beam or elastically scattered particle number (N_{el}). Thus the number of reaction events and the derived total reaction cross section were unaffected by dead time [see Eq. (1)].

Counter 3 (placed at 0°) detected the total residual beam. The high counting rate registered in this counter (almost equal to the incident beam intensity) did not allow event by event recording. We excluded these beam particles by setting an analog window on the TOF spectrum of detector 3 which included both the residual beam and the elastically scattered particles. The rejection of these events from computer acquisition was achieved by a fast anticoincidence unit which (within a 2 ns resolution) defined the following function:

$$F' = F \times \bar{3} , \tag{3}$$

which was stored by a scaler. Thus the real computer acquisition rate was F', which closely corresponds to the sum of the number of reaction events N_{reac} (after a small correction) and the number of particles elastically scattered out of counter 3 (obtained off line). Following this procedure each event was individually analyzed.

The TOF and the light output (L) signals from the 19 downstream detectors were sent, respectively, to a time-to-digital and a charge-to-digital converter (CAMAC). This information was then recorded on magnetic tape for off-line analysis. Additional information from counters 1 and 2 were also stored by scalers in order to continuously verify the acceptability of the measurement conditions during each run.

D. Beam optics

Our experiments were performed at several different European heavy ion accelerators (SARA at Grenoble, the S.C. at CERN, and SATURNE at Saclay). We required a very low beam intensity for these experiments ($\approx 10^4$ ps^{-1}); a similar procedure was employed to obtain such low intensities from each accelerator. This was simply achieved by closing appropriate pairs of slits located close to the beam extractor. Reaction products from slit scattering were eliminated by the following dipole and quadrupole magnets before reaching the target. During the experiment, the beam optics were optimized by using the counting rates of counter 1, collimator 2, and the six counters of ring 4. The ratio of counting rates of counters 2 and 1 was minimized; typical values were $\leq 5\%$. The individual rates of counters $4i$ (in cylindrical geometry) were continuously used to test for good beam alignment.

E. Targets

Accurate determination of the target thicknesses was of crucial importance. Therefore two independent methods were used to determine target thicknesses: (1) precise weighing of a measured area, and (2) alpha-particle energy loss. These two techniques gave consistent results. Special care was also devoted to the determination of target homogeneity. This was achieved by scanning the target surfaces during the alpha energy loss determinations. The thicknesses of the targets selected for this work ranged from 10 to 100 mg/cm^2, depending on the beam energy. Their corresponding uncertainties, including the inhomogeneity contribution, ranged between 2% and 8%. These target thicknesses were also chosen in such a way as to limit angular straggling to much less than the opening angle of the central detector 3.

Whenever the target thickness was the most important contribution to the error, an independent measurement of σ_R was performed with various thicknesses. These studies were mainly performed for the reaction $^{12}C + ^{12}C$.

III. DATA HANDLING AND EXPERIMENTAL RESULTS

The short exposure times needed (a few hours) and the complete autonomy of our setup permitted the completion of many systematic measurements at several different accelerators. Results for ≈ 45 values of σ_R are given in Tables I and II.

Target-in and target-out measurements were always performed. This procedure was necessary because counters 1 and 3 also act like targets. Thus, by subtracting the number of reaction events (normalized to the incident beam intensity) with and without the target, one could obtain the real contribution from the desired total reaction cross section.

A. Raw σ_R values

Off-line analysis of the recorded data led in a first step to values of σ_R(raw) (or uncorrected quantities). They are listed in the first column of Table I.

These quantities were obtained by using the electronic functions F and F' from the scalers (see Sec. II C). These values represented, respectively, the number of incident particles, N_{inc}, and the corresponding number of events recorded. The particles which reached counter 3 in a narrow window of time of flight centered on the beam velocity were rejected from the acquisition. Consequently, F' values were almost equal to the difference between the number of incident particles, N_{inc}, and the corresponding number of elastically scattered particles for angles within the central detector.

To determine σ_R from Eq. (1), we must determine the total number of particles elastically scattered out of the detection range of counter 3. This was partially achieved by using two dimensional plots (L-TOF) for the 18 detectors in rings $4i$ and $5j$. In each of these plots we integrated the number of events from the elastic peak, and corrected for the dead spaces due to the supports placed between each detector of the same ring. Due to the radial symmetry of these dead areas, this was simply achieved from the ratio of the dead to the active areas. The resulting number N_{el} $(\theta_3 < \theta < \theta_5)$ was then subtracted from F' to give σ_R(raw),

$$\sigma_R(\text{raw}) = \frac{[F' - N_{\text{el}}(\theta_3 < \theta < \theta_5)]}{F} \frac{A}{e\mathcal{N}} . \quad (4)$$

The errors associated with σ_R(raw) in Table I include statistical uncertainties, as well as those from the target thickness and the detection efficiency.

In the following subsections we explain how the additional corrections to σ_R(raw) were estimated. We restrict the discussion to the main principles for the sake of simplicity. We also give in Table I these corrections for measurements performed at SARA with a ^{12}C beam of 30 MeV/nucleon.

B. Corrections linked to the geometrical efficiency

The integrated cross sections for large angle $(\theta > \theta_5)$ elastically scattered particles had to be evaluated. Because of the lack of experimental elastic scattering measurements, these corrections were evaluated from calculated elastic scattering cross sections. Two rather different computer codes were used: (1) a standard optical model code (SPI) with parameters extrapolated from fits to a few measurements in the intermediate energy range,[29,35,36] and (2) a microscopic model proposed by Chauvin *et al.*[51,52] which is "parameter free." The latter uses only the free nucleon-nucleon cross sections and the size (mean square radii) of the colliding nuclei, both from experiment.[53–55] The predicted differential cross sections for our systems were then integrated over the angles greater than the acceptance of our setup. This gives the correction labeled $C(\theta > \theta_5)$ in Table I.

The predictions of the codes (GKAROL and SPI) were also used to estimate the number of elastically scattered particles in the small dead area between the two rings of detectors $4i$ and $5j$ at the polar angle θ_4 (see Fig. 1). The resulting values of $C(\theta_4)$ are listed in Table I.

The errors associated with these two corrections [which were subtracted from σ_R(raw)] prevent our results being completely model independent. However, for some systems, experimental elastic scattering data were available[29,35] and these errors were much less important.

C. Corrections due to the identification of the particles

In our setup elastically scattered particles were identified by atomic number ($Z = Z_p$) and TOF. Some reaction products were not distinguishable from elastic scattering on this basis. The number of such particles was estimated

TABLE I. Compilation of σ_R values measured with ^{12}C 30 MeV/nucleon projectiles performed at the accelerator SARA. It details σ_R(raw) values, the different corrections mentioned in the text, and σ_R final results with their respective uncertainties.

Target	σ_R(raw)	C(3)	C(neutron)	C(inelastic)	$C(\theta_4)$	$C(\theta > \theta_5)$	σ_R (mb)
^{12}C	1253± 30	28±12	15± 8	30±12		10± 2	1316± 40
^{27}Al	1676± 70	36±20	24±15	42±25	16± 10	14± 8	1748± 85
^{54}Fe	2158±120	54±30	27±16	70±45	68± 40	56± 30	2185±140
^{57}Fe	2260±140	64±35	29±18	70±45	70± 40	57± 30	2296±160
^{64}Zn	2420±150	54±30	30±20	80±50	80± 50	72± 40	2432±170
^{66}Zn	2393±150	58±30	32±20	80±50	80± 50	72± 40	2411±170
^{68}Zn	2590±160	67±40	30±20	80±50	90± 55	75± 45	2602±170
^{89}Y	3065±180	54±30	25±15	100±60	320±200	200±120	2724±300
^{nat}Ag	4450±500	70±45	35±20	150±90	600±350	600±350	3505±750

and their cross sections were added to the raw values of σ_R.

First, we had to estimate the number of projectile isotopes (produced by fragmentation processes or neutron transfer reactions) that would enter our detector setup within the TOF window (1 ns) used for the integration of the elastic peak. This correction was derived by using the data obtained for particles reaching the detectors with the charge number Z_p-1. The number of these reaction products was integrated in the same TOF window. The result was then related to projectile isotope production via other studies of projectiles fragmentation.[56–59] This procedure depends on several assumptions and consequently led to large errors in the corrections listed in column *C*(neutron) of Table I.

The second type of particle that merges (within our resolution) into the elastic peak was produced by inelastic scattering and was unduly counted as elastic scattering. We had to estimate the number of these particles for the solid angle subtended by our experimental setup and the excitation energy domain related to the width of the integration TOF window of the elastic events. A correction was estimated from the few published experimental data in this energy range.[35,60–62] The assumptions used in the extrapolation of these data to our systems led to uncertainties of up to 60% in the corrections. These corrections are listed in Table I in the column labeled *C*(inelastic).

Similarly, column *C*(3) gives corrections applied to σ_R(raw) for reaction products that enter the central counter (3) in the time window of elastic scattering which were improperly rejected in the data acquisition. This correction was made by using the integrated reaction products registered by rings $4i$ and $5j$ for the same time window as for counter 3. The two differential cross section values thus obtained at angles θ_4 and θ_5 were then extrapolated to 0° and integrated over the solid angle subtended by detector 3.

TABLE II. Compilation of the total reaction cross sections measured in this work. All the values are expressed in mb.

Target	Projectile	E_{lab} (MeV/nucleon)	σ_R (mb)
^{12}C	^{12}C	9.33	1444± 50
^{12}C	^{12}C	83	965± 30
^{27}Al	^{12}C	83	1397± 40
^{40}Ca	^{12}C	83	1510± 60
^{54}Fe	^{12}C	83	1776±100
^{56}Fe	^{12}C	83	1791±150
^{57}Fe	^{12}C	83	1867±100
^{64}Zn	^{12}C	83	1935±130
^{66}Zn	^{12}C	83	2057±130
^{68}Zn	^{12}C	83	2145±130
^{89}Y	^{12}C	83	2124±140
^{12}C	^{12}C	200	864± 45
^{27}Al	^{12}C	200	1270± 70
^{nat}Fe	^{12}C	200	1648±110
^{nat}Zn	^{12}C	200	1747±110
^{89}Y	^{12}C	200	1885±120
^{nat}Ag	^{12}C	200	2183±170
^{12}C	^{12}C	250	873± 60
^{27}Al	^{12}C	250	1173± 90
^{nat}Fe	^{12}C	250	1595±120
^{nat}Zn	^{12}C	250	1738±145
^{12}C	^{12}C	300	858± 60
^{27}Al	^{12}C	300	1220± 85
^{nat}Fe	^{112}C	300	1575±110
^{nat}Zn	^{12}C	300	1710±125
^{89}Y	^{12}C	300	1885±150
^{nat}Ag	^{12}C	300	2202±160
^{27}Al	^{16}O	30	1724± 80
^{89}Y	^{16}O	30	2707±330
^{12}C	^{20}Ne	30	1550± 75
^{27}Al	^{20}Ne	30	2113±100
^{56}Fe	^{20}Ne	30	2769±190
^{64}Zn	^{20}Ne	30	2870±180
^{12}C	^{20}Ne	100	1161± 80
^{27}Al	^{20}Ne	100	1446±120
^{64}Zn	^{20}Ne	100	2162±200
^{12}C	^{20}Ne	200	1123± 80
^{12}C	^{20}Ne	300	1168±100
^{27}Al	^{20}Ne	300	1328±120
^{nat}Ag	^{20}Ne	300	2407±200

D. Final results for σ_R

Final values for σ_R were obtained after summing all the above corrections to σ_R(raw) (see Table I), and quadratically adding all the uncertainties. In Table II we have listed the final values of σ_R measured in this work. We can see that most of our measurements have accuracies between 4% and 8% with only small effects from the above corrections. However, for the heaviest systems the corrections do impose a real limitation to this measurements technique.

IV. COMPARISON WITH THEORETICAL MODELS

A. Strong absorption models

Strong absorption models were originally developed to describe low energy nuclear reactions. In this framework the total reaction cross section is simply calculated by considering that a reaction occurs whenever substantial contact occurs between nuclear matter. The σ_R values can be expressed[45] in terms of transmission coefficients $T(l)$ through a one dimensional potential barrier (D) calculated separately for each impact parameter (b) or angular momentum (l). It follows that

$$\sigma_R=\pi\lambda\!\!\!^{-2}\sum_{l=0}^{\infty}(2l+1)T(l)\ , \tag{5}$$

$\lambda\!\!\!^{-}$ being the associated projectile reduced wavelength.

Within the sharp cutoff approximation [$T(l)=1$ for $l<l_{crit}$; otherwise, $T(l)=0$], one obtains

$$\sigma_R=\pi\lambda\!\!\!^{-2}(l_{crit}+1)^2=\pi R_{int}^2[1-(D/E_{c.m.})]\ , \tag{6}$$

where R_{int} is the strong absorption radius and D is the l-

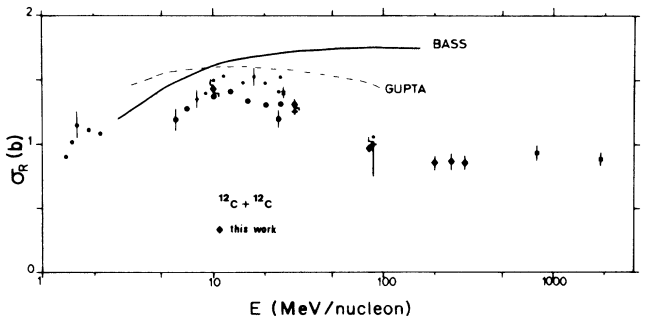

FIG. 3. Total reaction cross section for $^{12}C+^{12}C$ as a function of incident energy. Data points are from Refs. 25, 28–30, 33, 35, and 63. The solid and dashed curves are the results of parametrizations discussed in the text and are labeled by the author's name.

dependent potential barrier height.

From this relation one sees that σ_R saturates with increasing beam energy at the so-called geometrical value ($\pi R_{\rm int}^2$). Different expressions of this type have been derived by many authors; they differ in the way of parametrizing the radius $R_{\rm int}$ and the barrier D.[44–47]

In Fig. 3 the data are plotted for the $^{12}C+^{12}C$ system as obtained from various experimental techniques (see figure caption). The strong absorption model of Bass[45] is compared to the experimental results. It is clear that the observed decrease of σ_R deviates significantly (above 20–30 MeV/nucleon) from the geometrical limit predicted by this model. This is true for all strong absorption models. Gupta's calculations are partially successful in reproducing the decrease in σ_R at energies around 20 MeV/nucleon, but they fail to describe the variation of σ_R over the whole energy range.

One may, therefore, conclude that strong absorption models do not include the basic physical features which give the decrease of σ_R with energy in this energy range.

B. Microscopic models

Several microscopic models have been developed to account for data in the high energy range.[4–11] We briefly review their basic concepts in this paragraph.

In these models nuclear reactions are described in terms of a sum of individual nucleon-nucleon (N-N) scattering processes. Thus, for a nucleon-nucleus collision, the physical ingredients of such calculations are simply (i) the matter density distribution of the target, and (ii) and N-N total scattering cross sections ($\sigma_T^{\rm NN}$). These quantities are used to construct a local mean free path:

$$\Lambda(r)=[\rho(r)\sigma_T^{\overline{\rm NN}}]^{-1}\ , \tag{7}$$

with $\rho(r)$ the target nuclear matter density and $\sigma_T^{\overline{\rm NN}}$ the N-N total scattering cross section averaged over isospin.

In nucleus-nucleus collisions the mean free path of the projectile is obtained by averaging over the mean free path of the different incident nucleons in the target. This is achieved by constructing the volume overlap of the interacting nuclei. At a given distance r between the centers of the colliding nuclei, the local mean free path of the projectile in the target is given by

$$\Lambda(r)=\left[\sigma_T^{\overline{\rm NN}}\int d\tilde{r}\int_V \rho_p(\mathbf{s})\rho_t(\mathbf{r}-\mathbf{s})d\mathbf{s}\right]^{-1}\ , \tag{8}$$

$\sigma_T^{\overline{\rm NN}}$ being the isospin averaged N-N total cross section and $\rho_{p\ (t)}$ being, respectively, the nuclear density distributions of the projectile and target; V is the nuclear volume overlap at the distance r, s is the position variable for the integration over the overlap volume, and $d\tilde{r}$ is the angular part of variable $\mathbf{r}$.

After integrating the local mean free path over the whole trajectory of the projectile, one obtains the probability for no N-N interaction [$T_0(b)$] at a given impact parameter (b). This quantity can be expressed as

$$T_0(b)=\exp\left[\int_{-\infty}^{+\infty}-\frac{dz}{\Lambda(r)}\right]\ . \tag{9}$$

The distance with respect to the beam axis is z and thus $r^2=b^2+z^2$.

Within this microscopic model, σ_R is then derived by assuming that any N-N scattering process leads to a nuclear reaction event between the complex colliding nuclei. Under this assumption, σ_R is related to $T_0(b)$ by the following relation:

$$\sigma_R=\int_0^{\infty}2\pi b[1-T_0(b)]db\ . \tag{10}$$

As these microscopic models were first developed for the relativistic energy range, straight-line trajectories were often assumed for the projectile. Also, total cross sections for free N-N scattering were generally employed. However, some authors also took into account the Pauli exclusion principle (Pauli "blocking") and/or the Fermi motion.[64–66] Nuclear matter distributions were generally assumed to be identical to charge distributions measured by electron scattering experiments.[54,55] Obviously, this assumption neglects any differences between the neutron and proton distributions.

We will now describe the microscopic model we have used for this analysis.

1. *Karol's microscopic model*

Karol[10] has derived an analytic expression for σ_R by assuming a simple Gaussian shape for the nuclear matter density distributions. Its shapes were deduced semiempirically to reproduce the tails of the nuclear matter distribution. His results are similar to microscopic calculations performed with realistic matter distributions. This is explained by the fact that the σ_R variations are mainly governed by the most peripheral collisions and thus related to the nuclear surface shapes. The analytical expression for the probability of zero N-N collision at a given impact parameter (b) is given by

$$T_0(b)=\exp\left[-\frac{\pi^2\sigma_T^{\overline{\rm NN}}\rho_t(0)\rho_p(0)a_t^3a_p^3}{a_t^2+a_p^2}\times\exp\left[-\frac{b^2}{a_t^2+a_p^2}\right]\right]\ . \tag{11}$$

Symbols $a_{p\,(t)}$ and $\rho_{t\,(p)}(0)$ represent the Gaussian shape distributions of projectile and target (see Ref. 10 for detailed expressions and calculations).

We have slightly modified Karol's formalism to include deflection of the projectile, which can be important at subrelativistic energies. Following DeVries *et al.*,[12] $T_0(b)$ in Eq. (10) was replaced by $T_0(b')$, where b' is the classical distance of closest approach of the projectile in the Coulomb plus nuclear potential. The values of b' were obtained for each impact parameter in the framework of classical trajectory calculations. Now σ_R can be obtained from the following expression:

$$\sigma_R = \int_0^\infty 2\pi b[1-T_0(b')]db \ . \tag{12}$$

In these calculations the nuclear potential has been obtained from the real part of an optical potential extracted by an analysis of elastic scattering for reaction systems close to ours.[29,35,36] One should emphasize at this point that Coulomb repulsion usually dominates the projectile trajectory. For the lightest projectiles the effect of the nuclear potential is important,[14] and can significantly counterbalance the Coulomb repulsion. Therefore, a more careful treatment was needed.

We have neglected Pauli "blocking" and Fermi motion. The effect of a neutron skin was also neglected. The importance of these aspects will be discussed later.

C. Comparisons between data and calculations

We first applied this model to the reaction $^{12}C+^{12}C$. Figure 4 shows the variation of σ_R as a function of beam energy. We show only the data obtained by direct measurement techniques.[25,38] The microscopic model predictions are represented by a solid line; they show excellent agreement with the experimental results over the whole energy range. Comparable agreement was previously obtained for lighter projectiles.[12,31] In the framework of this microscopic model, the variation of σ_R is linked to the individual N-N total cross section behavior as represented at the bottom of Fig. 4. We note that the calculated decrease for σ_R below 15 MeV/nucleon is dominated by Coulomb repulsion. In Fig. 5 we show σ_R data at 30 and 300 MeV/nucleon for a wide range of masses. The data are plotted as a function of $(A_p^{1/3}+A_t^{1/3})^2$, which is essentially proportional to the strong absorption radius.[44–46] Figure 5 shows an approximately linear dependence of σ_R on $(A_p^{1/3}+A_t^{1/3})^2$, but the slope is energy dependent. There is a decrease of $\approx 40\%$ in σ_R when the beam energy is increased from 30 to 300 MeV/nucleon [corresponding to a variation of $\approx 20\%$ in the strong absorption radius from Eq. (6)]. This decrease is globally reproduced by the microscopic calculations over the whole mass range. We note that the decrease observed for σ_R corresponds to a variation from 300 to 60 mb for the total averaged N-N scattering cross section in the same energy range.

Thus, in the framework of this model, the origin of the decrease in σ_R can be understood in terms of an increasing "transparency" effect in N-N collisions. This means that nuclear matter has become transparent for these nuclear interactions at certain impact parameters when the beam energy increases. These impact parameters can be inferred from the analytical transparency function $T_0(b)$ as expressed in Eq. (11). Figure 6 displays this calculated

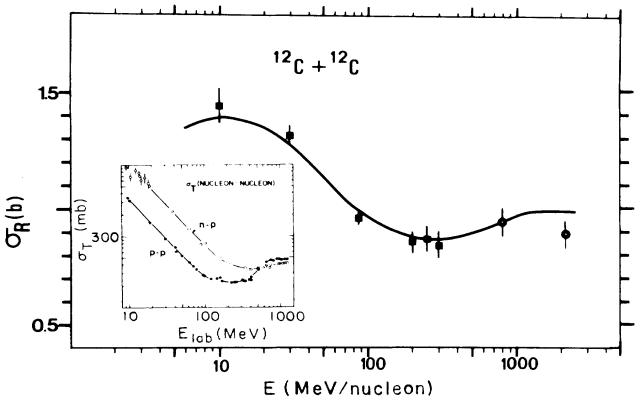

FIG. 4. Measurements of the $^{12}C+^{12}C$ total reaction cross section from direct measurement techniques. The solid squares represent our data, and the two circles at >500 MeV/nucleon are from Ref. 25. The solid line is from the microscopic model calculation discussed in Sec. IV B. Nucleon-nucleon total cross sections (from Ref. 53) are shown in the inset.

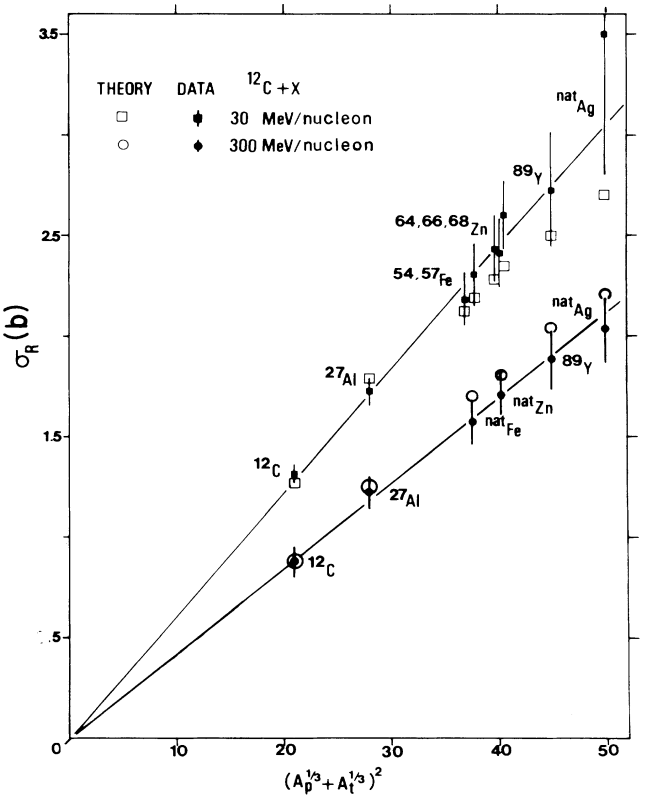

FIG. 5. Measured total reaction cross sections (this work) from ^{12}C at 30 and 300 MeV/nucleon. The transparency effect (a systematic decrease in the measured values of σ_R as the energy increases) is clearly observed. The target is indicated; straight lines are drawn to guide the eye. Predictions of the microscopic model are represented by open symbols.

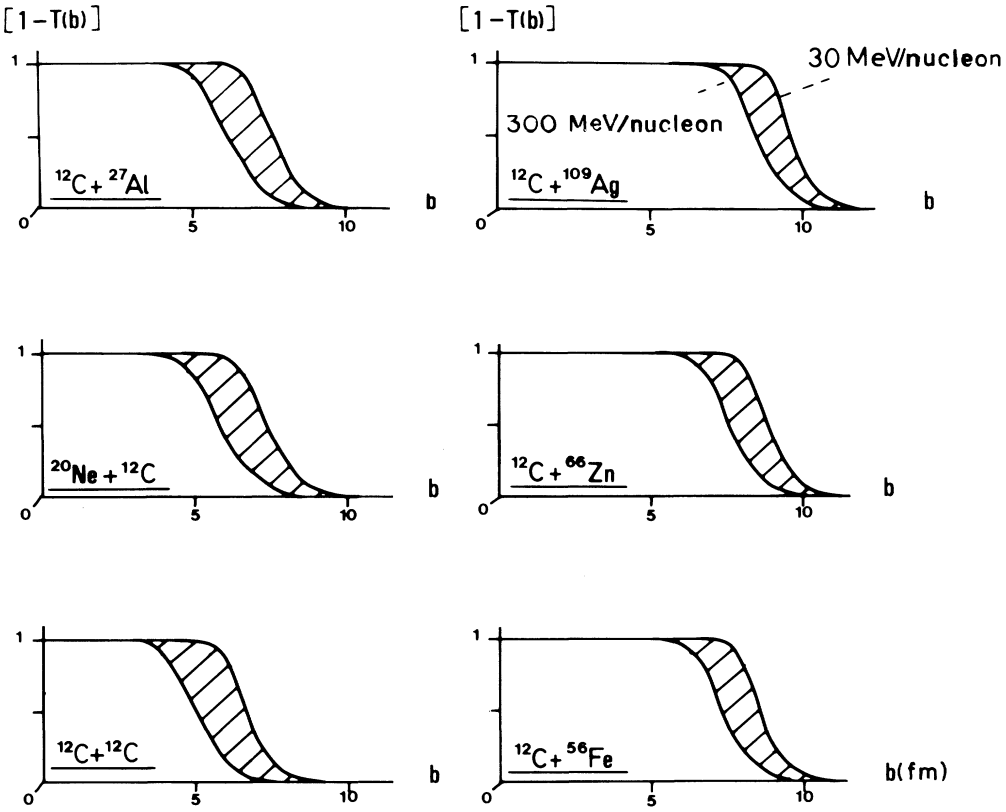

FIG. 6. Modification of the absorption probability with energy in the microscopic model. The figure shows that the predicted transparency effect is confined to a 1.5 fm band in the impact parameter on the surface of the reaction sphere, for an energy increase from 30 to 300 MeV/nucleon.

quantity as a function of the impact parameter for different systems at 30 and 300 MeV/nucleon. This figure shows that only the most peripheral collisions are affected by the decrease of the N-N total cross section, even at 300 MeV/nucleon, where the transparency effect is rather strong. Thus the decrease in σ_R is due to surface transparency, implying that this quantity σ_R does not give direct information on the more central collision processes.

Figure 7 illustrates the behavior of σ_R in the region of 80—300 MeV/nucleon. The trend of our data suggests that a minimum in σ_R is located at $\approx$300 MeV/nucleon independently of the mass of the colliding system. This observation excludes any presence of strong coherent effects in the pion production and suggests that the variation of σ_R in the energy region 100—300 MeV/nucleon is governed by individual N-N collisions.

Another point of interest is the so-called isotopic effect, which strongly influences the σ_R data previously obtained with the proton's projectile.[22] In these cases it was observed that σ_R increases abruptly with neutron excess for a given element ($\approx$20% variations for a change of a few nucleons in targets from Ni to Zn). In our work we studied the isotopes of iron (^{54,56,57}Fe) and zinc (^{64,66,68}Zn) with a ^{12}C beam at two different energies, in order to search for this effect in heavy ion collisions. Figure 8 displays the results. The solid lines are drawn to illustrate

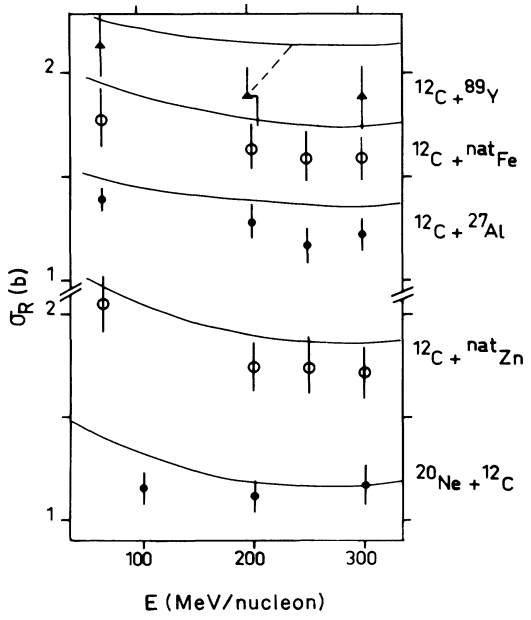

FIG. 7. Total reaction cross section measurements as a function of incident energy. The solid lines are predictions of the microscopic model as discussed in the text.

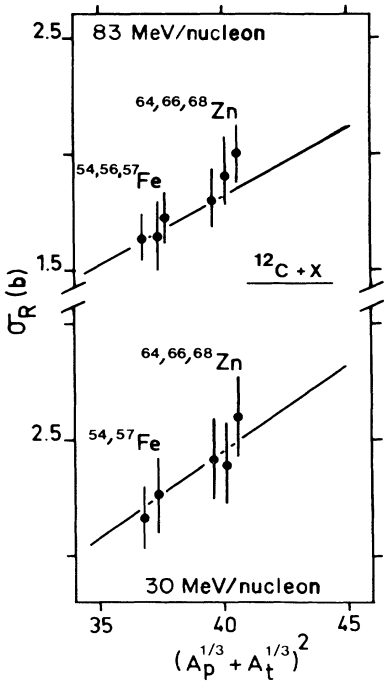

FIG. 8. Isotopic dependence for measured values of σ_R (see Sec. IV C). As can be seen in the figure, the effect appears to be small and needs more accurate measurements.

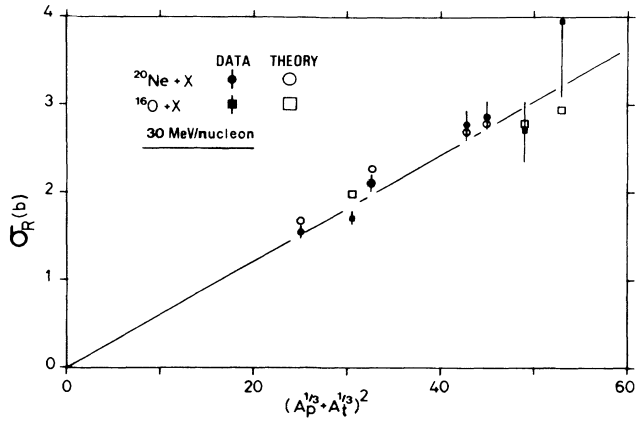

FIG. 9. Total reaction cross sections for ^{20}Ne and ^{16}O induced reactions at 30 MeV/nucleon compared to predictions of the microscopic model.

the generally linear dependence of our data with increasing mass as a function of $(A_p^{1/3}+A_t^{1/3})^2$. Small deviations from the linear dependence can be seen for the zinc isotopes; however, they seem to be within the uncertainties (mainly from target thickness inhomogeneities). More precise results are needed to obtain a clear view of possible isotopic effects in the variation of σ_R for heavy ion collisions. The origin of such a dependence may be understood in the framework of Karol's microscopic model if one allows for a neutron skin located at the nuclear surface and recalls that below 200 MeV/nucleon the free N-N total cross section is about 3 times greater in the proton-neutron (n-p) than in the p-p and n-n collisions.[53] For the proton projectile, collisions with the neutron rich skin of the target (occurring at large impact parameters) should play an important role for the reaction cross section. However, in heavy ion collisions the isotopic effect is washed out as one has to deal also with the neutrons of the projectile. In addition, for heavy projectiles the reactions occurring at the surface represent a smaller fraction of the total reaction cross section. We thus have to consider quantities which are more specific than σ_R to elucidate the influence of the neutron rich skin in heavy ion collisions. Harvey[58] has performed a study of the isotopic distribution of the fragmentation products at two energies (below and above 200 MeV/nucleon). He clearly demonstrated that the experimental yields could be described well by using this physical concept. We will describe, in the next subsection, how we have introduced a neutron skin effect into Karol's formalism.

We have also investigated the dependence of σ_R on projectile mass. Figures 9 and 10 show results with projectiles ranging from ^{1}H to ^{20}Ne at the same incident energy per nucleon (30 MeV/nucleon). If one only considers our data, no significant difference is observed for projectiles ranging from ^{12}C to ^{20}Ne (Fig. 9). On the contrary, for a larger range of projectile masses that includes lighter ones,[12,22] a strong dependence clearly appears (Fig. 10). In fact, in this figure a nearly linear dependence of σ_R on $(A_p^{1/3}+A_t^{1/3})^2$ is observed with a slope that depends on the projectile mass. An important point concerns the fact that for a given value of $(A_p^{1/3}+A_t^{1/3})^2$ a maximum for σ_R is observed at the mass symmetry of the colliding system. As these data were obtained at the same incident energy per nucleon, this effect cannot be attributed to a transparency phenomenon for individual N-N collisions. This mass asymmetry effect was previously pointed out and accounted for within the framework of a microscopic model.[34] The number of N-N collisions that occurs during a nuclear reaction depends on the volume overlap of the colliding nuclei, which, for a given radial separation of projectile and target, has a maximum for mass symme-

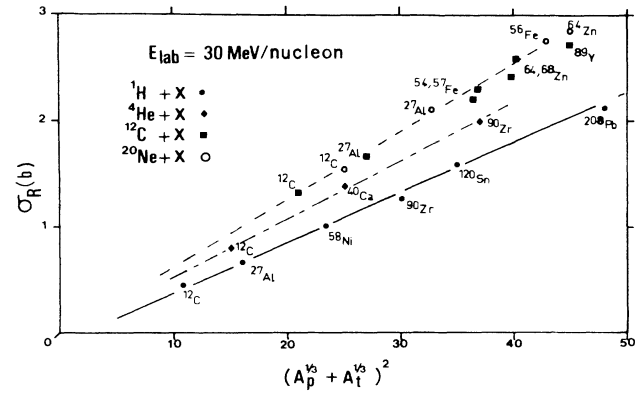

FIG. 10. Data of Refs. 12 and 22 and of this work illustrating the effect of projectile-target asymmetry on measured values of σ_R at 30 MeV/nucleon.

try in the entrance channel. This leads to a higher value of σ_R, in agreement with the observations shown in Fig. 10. We note that new data for heavier projectiles (Ar, Kr, and Xe) at the same bombarding energy per nucleon would be of great interest to complete such a study.

In this subsection we have shown a general agreement between experiment and a microscopic model based on Karol's formalism. However, some deviations remain, and the next subsection will be devoted to their explanation in terms of additional physical effects.

D. Deviations from predictions of the microscopic model

1. Role of the neutron rich skin in collision between nuclei

In the preceding subsection we saw that some experimental results suggest an important role for the neutron-rich skin, especially for the heaviest targets. In order to test this hypothesis, we have introduced a neutron-rich skin into Karol's formalism by using Myers's parametrization[67] for the difference between the mean radii of the distributions of neutrons and protons. This leads to four separate terms instead of one in Eq. (11), as we consider different distributions for neutrons and protons. The resulting contributions to the transparency $T_0(b)$ remain analytical, as we still follow Karol's procedure. The root mean square (rms) radii of these distributions were taken from the Myers's prescription.[67] This choice introduces differences of a few percent in the radii as compared to those empirically determined by Karol using only the charge distribution of nuclei. The resulting calculated values of σ_R are increased by about 1—3 % for our systems. For heavier targets this increase can be $\approx 5\%$ for a proton projectile.

One must recall that Myers's parameters refer to the mean isotopic mass of each nucleus. We thus had to make additional assumptions to account for the observed isotopic effects in σ_R. For a given nucleus (projectile or target) the difference between proton and neutron radii was taken from the Myers prescription for a nucleus, which had (on average) the same neutron to proton ratio. With these assumptions we obtain a 2—4 % variation in σ_R for the isotopes studied by Menet *et al.*,[22] with an additional 2—4 % for changes in the nuclear potential with increasing neutron excess. This second effect was calculated by using the real part of the optical potential given by Menet *et al.*[22] All these results indicate that consideration of the neutron rich skin may reduce the deviations between experiment and calculation at energies less than 100 MeV/nucleon. However, the use of these more realistic matter distributions and optical potentials cannot account for all the experimentally observed isotopic effects. Thus one may also need to consider contributions of collective effects, such as static deformations, to explain the remaining discrepancies.

2. Fermi motion and Pauli "blocking" effects

In microscopic models the nucleons that collide in the volume overlap of the interacting nuclei are generally considered to be in free motion. However, the average effect of the other nucleons is considered in two ways. First, the internal motion of the nucleons in the nuclei implies that the N-N collisions do not occur only at the incident beam energy per nucleon. Second, the Pauli exclusion principle forbids a N-N collision whenever the two colliding nucleons are not scattered into unoccupied states. These two combined effects reduce the values of σ_R as shown by DiGiacomo *et al.* for N-nucleus interactions.[65,66] For heavy projectiles these authors have derived an effective cross section for the N-N scattering ($\sigma_{T\,\mathrm{eff}}^{\mathrm{NN}}$) in the volume overlap of the colliding nuclei.[66] More refined calculations may be available,[18] but those from Ref. 66 are probably sufficient to describe the general trends of the σ_R variation. In a simple Fermi gas model, the radius of the Fermi sphere is related to the nuclear density. Consequently, at the nuclear surface, the local Fermi distribution has a reduced radius (in momentum space) and so the Pauli exclusion effect is strongly reduced. In Fig. 11 we show a calculated profile of the density overlap of two colliding nuclei. This is drawn for a case where the distance between the nuclear centers is equal to their closest distance of approach [for an impact parameter b_0 that gives $T_0(b_0)=0.5$]. In Fig. 11 one can see that only the extreme tails of the matter distributions are involved in such heavy ion collisions. Thus at 30 MeV/nucleon, these densities represent around $\frac{1}{16}$ of their central values, leading to local Fermi sphere radii (K_F) of about 0.6 fm^{-1} compared to 1.5 fm^{-1} for the central region. We should point out that the densities in the nuclear overlap are even smaller for heavier target masses. The extrapolation of $\sigma_{T\,\mathrm{eff}}^{\mathrm{NN}}$ (calculated by DiGiacomo *et al.*[66] for $K_F=1.5$ and 0.75 fm^{-1}) shows at 30 MeV/nucleon a threefold reduction of $\sigma_{T\,\mathrm{eff}}^{\mathrm{NN}}$ as compared to that for free nucleon collisions. This reduction seems to be very strong; however, the resulting σ_R values decrease by only 15%. Following

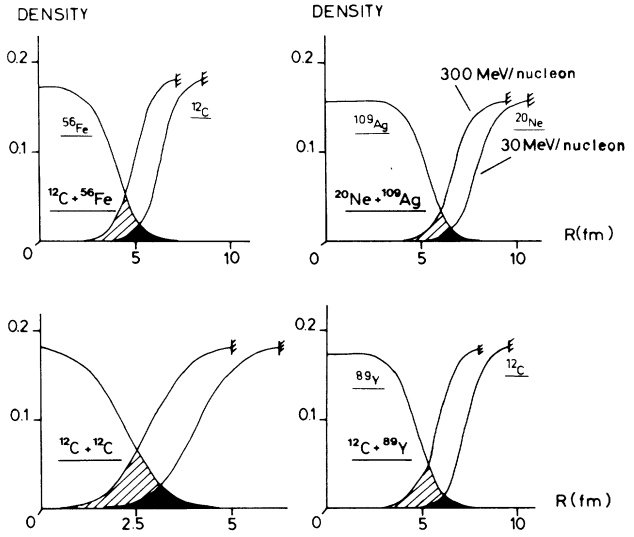

FIG. 11. Projectile and target matter-density distributions for various systems, drawn at a radial separation corresponding to the distance of closest approach for a trajectory in which the transparency $T_0(b)=0.5$. The figure illustrates typical density overlaps that are important in the calculation of σ_R (see text).

the same procedure, we obtain a reduction of $\approx 8\%$ in σ_R at 83 MeV/nucleon and $\approx 3\%$ at 300 MeV/nucleon. This estimate is very crude; nevertheless, it allows us to draw some qualitative conclusions. The Pauli "blocking" effect seems to improve the agreement with the high energy data (around 300 MeV/nucleon), as shown in Fig. 7, but worsens the deviations observed for the heavier targets at 30 MeV/nucleon. The experimental decrease of σ_R with energy becomes stronger than predicted by the microscopic calculation if all these effects (neutron skin and Pauli "blocking") are included. This trend can also be similarly reproduced if one includes either nuclear collective effects (which are observed to vanish also at high energy[18,35]) or an important neutron rich skin effective or both.

We conclude that the main trends of σ_R in the intermediate energy range can be understood in terms of geometric and microscopic quantities. However, nuclear structure or isotopic effects may contribute significantly for heavy systems.

V. A NEW PARAMETRIZATION FOR σ_R

Macroscopic phenomenological models, developed in the framework of the strong absorption hypothesis, fail to describe the behavior of σ_R. Transparency and mass asymmetry effects are observed in our work at intermediate bombarding energies. As a microscopic model has succeeded in a general globally description of our experimental results, it appears that any new parametrization of σ_R should include the physical content of this model.

We have previously reported[39] a phenomenological parametrization for σ_R. In this section we will review the physical meaning of its different terms and propose an additional term introduced to describe the trends of recently measured data for heavier systems.[36,37,40] We begin by writing the equation

$$\sigma_R = \pi R_{\rm int}^2 \left[1 - \frac{B_C}{E_{\rm c.m.}} \right] , \tag{13}$$

where the term B_C is the Coulomb barrier of the projectile-target system. It is given by

$$B_C = \frac{Z_t Z_p e^2}{r_C (A_t^{1/3} + A_p^{1/3})} , \tag{14}$$

with $r_C = 1.3$ fm, $Z_{p\,(t)}$ are the atomic numbers of target and projectile nuclei, $A_{p\,(t)}$ are their mass numbers, and $R_{\rm int}$ is the interaction radius. We propose to divide this latter quantity into volume (vol) and surface (surf) terms,

$$R_{\rm int} = R_{\rm vol} + R_{\rm surf} . \tag{15}$$

In Sec. IV we have shown that collisions occurring at the smaller impact parameters give rise to nuclear reactions independent of energy and mass. This result can be parametrized as a volume (or core) component of the interaction radius. It is given by

$$R_{\rm vol} = r_0 (A_p^{1/3} + A_t^{1/3}) . \tag{16}$$

This is similar to the interaction radius in the black disk model for low bombarding energies, but with values of r_0 reduced by about 20% as compared with those for low energies.

The second component of the interaction radius is a nuclear surface contribution which we propose to parametrize in the following way:

$$R_{\rm surf} = r_0 \left[a \frac{A_p^{1/3} A_t^{1/3}}{A_p^{1/3} + A_t^{1/3}} - c \right] . \tag{17}$$

The first term in the large parentheses is the mass asymmetry term, which is related to the volume overlap of projectile and target, and c is an energy dependent parameter which takes care of increasing surface transparency as the projectile energy increases.

The surface component of the interaction radius ($R_{\rm surf}$) was introduced to reproduce the trends of our experimental data at intermediate energies. Our radius thus has two distinct contributions based on two distinct physical effects (mass asymmetry and transparency). As mentioned above, these trends cannot be described in the framework of the strong absorption model.[44–46]

The values of the parameters of our parametrization have been fixed by using a χ^2 minimizing procedure. We used a set of more than 100 values of σ_R measured between 30 and 2100 MeV/nucleon with projectiles ranging from ^{1}H to ^{40}Ar and targets ranging from ^{9}B to ^{208}Pb. The parameters r_0 and a were uniquely fixed for all the studied systems, while the parameter c was allowed to vary only with the beam energy per nucleon. The best χ^2

TABLE III. Shows r_0, a, and c values extracted from the best χ^2 fit of σ_R data with our semiempirical parametrization.

Projectile	$E_{\rm lab}/A$ (MeV/nucleon)	r_0 (fm)	a (dimensionless)	c (dimensionless)	Data references	χ^2/N [using formulas (13)–(17)]	χ^2/N [using Eq. (18)]
^{1}H, ^{4}He, ^{12}C, ^{16}O, ^{20}Ne	30	1.1	1.85	0.65	this work, 12, 22, 31	3.5	1.4
^{1}H, ^{40}Ar	40–44	1.1	1.85	1.2	22, 38, 40	2.8	1.2
^{1}H, ^{12}C, ^{40}Ca	77–83	1.1	1.85	1.65	this work, 23, 40	2	2
^{1}H, ^{12}C, ^{20}Ne	200–300	1.1	1.85	2.05	this work, 23	1.5	1.5
^{1}H, ^{2}H, ^{4}He, ^{12}C	900–2100	1.1	1.85	1.9	25	0.8	0.8

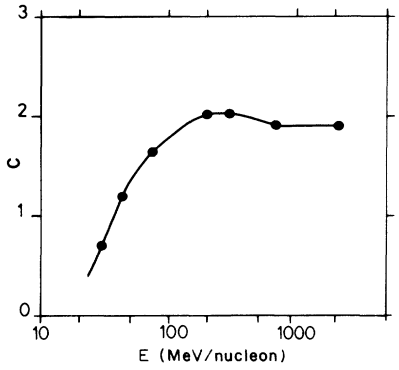

FIG. 12. Variation of the semiempirical parameter c (see Sec. V) as a function of incident energy.

fit provided the following value: $r_0 = 1.1$ fm and $a = 1.85$, while the corresponding values of c are listed in Table III for each projectile energy per nucleon. The normalized χ^2 values obtained with these sets of parameters are ≈ 2. This means that most of the measured σ_R values could be predicted within $\approx 10\%$. One notes that the fitted values of c vary smoothly with energy as shown in Fig. 12. This observation tends to increase the confidence in our semiempirical parametrization.

However, for the heaviest or neutron rich target the predictions seem to underestimate the experimental values (especially for the proton projectile). One possible way of explaining this discrepancy involves a neutron-skin excess. We have therefore modified the parametrization described above to explicitly include a neutron skin for the target. Equation (17) has been changed as follows:

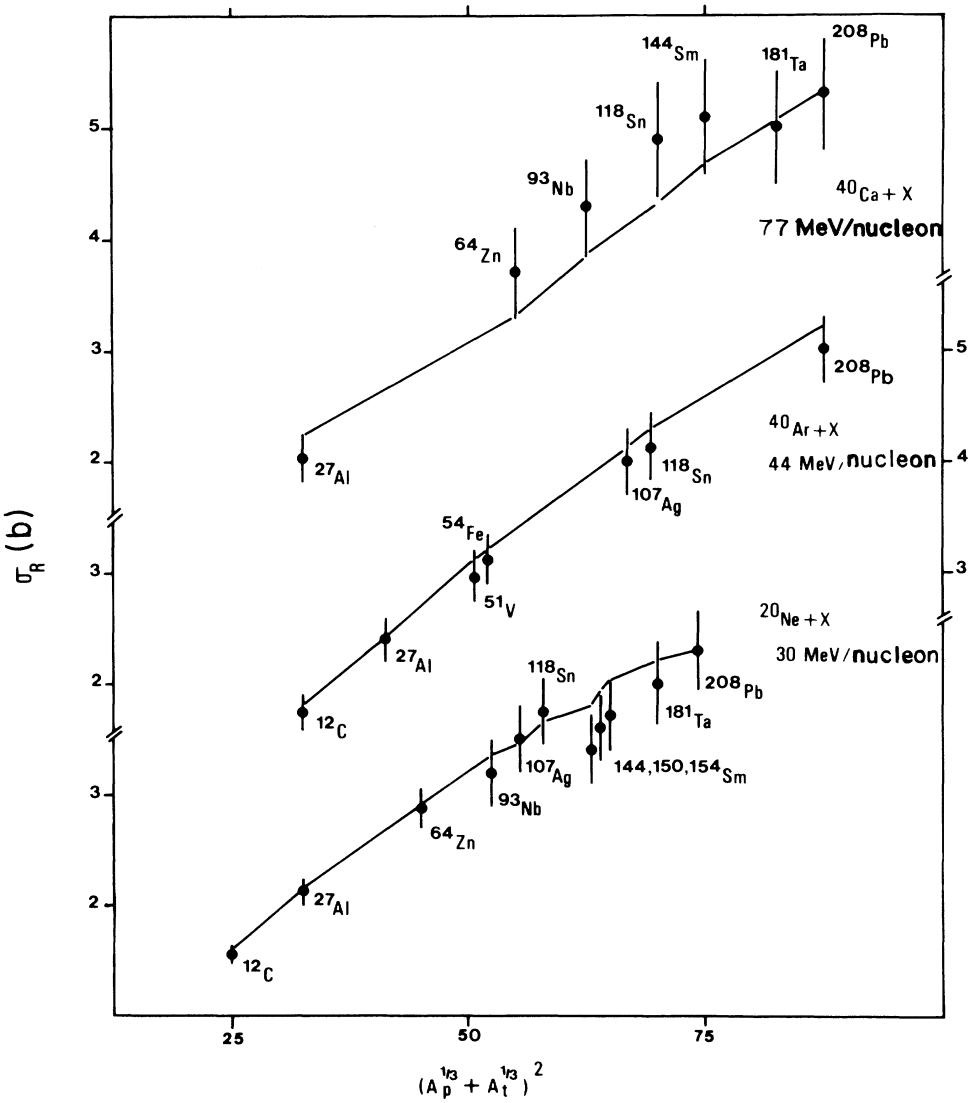

FIG. 13. Total reaction cross sections for 30 MeV/nucleon ^{20}Ne, 44 MeV/nucleon ^{40}Ar, and 77 MeV/nucleon ^{40}Ca induced reactions as a function of $(A_p^{1/3} + A_t^{1/3})^2$, compared with the predictions of the semiempirical parametrization proposed in this work (solid lines). These data are taken from Ref. 40 and have been measured by using the techniques of direct "associated α rays with 4π detection."

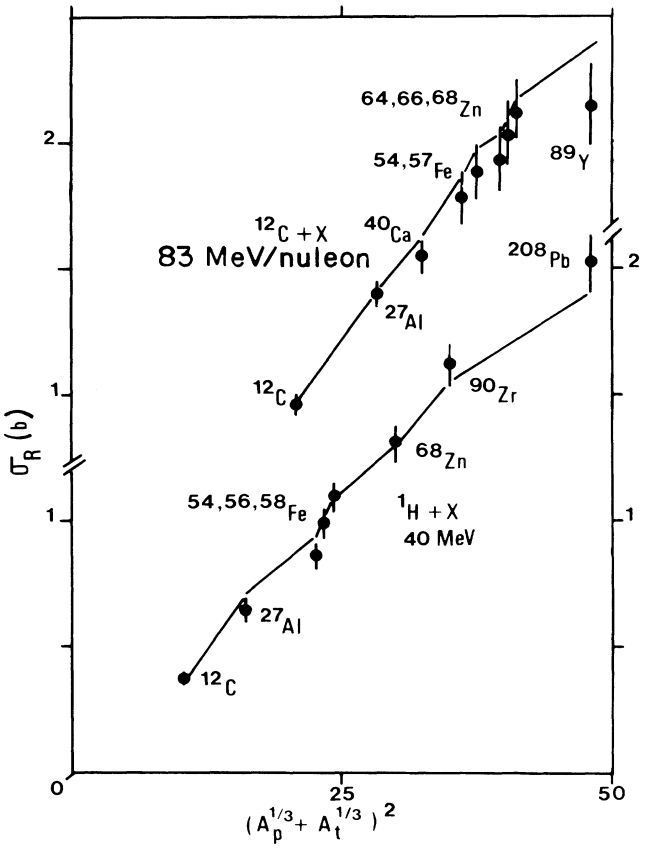

FIG. 14. Same as Fig. 13, but for ^{12}C of 83 MeV/nucleon (this work) and protons of 40 MeV (Ref. 22) projectiles.

$$R_{\text{surf}} = R_{\text{surf}} + D \ , \tag{18}$$

where the new neutron excess term D can be expressed as

$$D = \frac{5(A_t - 2Z_t)Z_p}{A_p A_t} \ . \tag{19}$$

The factor 5 has been derived using a χ^2 minimizing procedure. This modification acts only below 200 MeV/nucleon [above this energy, the total cross section for neutron-proton (n-p) collisions becomes equal to those of n-n or p-p collisions[53]].

With this additional term (D) and without any changes in the previously derived values of the parameters r_0, a, and c, the final normalized value of χ^2 was decreased from 2 to 1.5 (see Table III). A comparison between data taken from Refs. 22, 37, 38, and 40 and the predictions of this parametrization is shown in Figs. 13 and 14. Even though some discrepancies still remain, we note very good overall agreement. This indicates that our parametrization does account for the main aspects of the behavior of σ_R at energies above 300 MeV/nucleon.

VI. SUMMARY AND CONCLUSIONS

In this work we have summarized the first direct systematic measurements of heavy ion total reaction cross sections performed in the intermediate energy range. The variation of σ_R with energy has been measured for a wide variety of projectile-target combinations. A decrease of σ_R with increasing energy above 30 MeV/nucleon is observed. A minimum is also suggested for σ_R at ≈ 300 MeV/nucleon independent of mass. Low-energy, strong-absorption models fail to reproduce this variation of σ_R as a function of the bombarding energy. On the contrary, the predictions of a simple microscopic model (originally developed by Karol,[10] and slightly modified here) reproduce well the general trends of our data. This agreement seems to link the dependence of σ_R on projectile energy to the behavior of the N-N total cross section. As Pauli "blocking" and Fermi motion effects have not been fully included in such calculations, one cannot exclude the possibility that part of this decrease could be connected to the disappearance of macroscopic surface excitation modes with increasing energy.[18] The mass asymmetry dependence of σ_R has been simply explained in the framework of this microscopic model by using a pure geometrical argument. However, the prediction of this model seems to systematically underestimate recently measured σ_R values.[40] These discrepancies may be related to some incorrect evaluation of the Coulomb plus nuclear potential effects or due to nuclear structure effects (e.g., collective deformations or excitations, neutron skin effects).

All these effects are taken into account in a consistent way in the derivation of a new expression for σ_R for the intermediate range. The improvements of this parametrization over those previously proposed are twofold. First, we have based our formula on well identified physical concepts or quantities. Second, its predictions reproduce most of the measured data at energies higher than 30 MeV/nucleon with a very simple formula with a single energy-dependent parameter.

*Present address: Deutsches Elektronen-Synchrotron, Hamburg, Federal Republic of Germany.

†Also at Laboratoire National Saturne, 91191 Gif-sur-Yvette Cédex, France.

‡Present address: Faculte des Sciences, Université de Rabat, Rabat, Morocco.

[1]H. A. Bethe, Phys. Rev. **57**, 1125 (1940).

[2]S. Fernbach, R. Serber, and T. B. Taylor, Phys. Rev. **75**, 1352 (1949).

[3]H. L. Bradt and B. Peters, Phys. Rev. **77**, 54 (1950).

[4]Y. Eisenberg, Phys. Rev. **96**, 1378 (1954).

[5]R. W. Williams, Phys. Rev. **98**, 1387 (1955).

[6]G. Alexander and G. Yekutieli, Il Nuovo Cimento **19**, 103 (1960).

[7]H. W. Bertini, Phys. Rev. **188**, 1711 (1969).

[8]H. W. Bertini, Phys. Rev. C **6**, 2118 (1972).

[9]S. Barshay, C. B. Dover, and J. P. Vary, Phys. Rev. C **11**, 360 (1975).

[10]P. J. Karol, Phys. Rev. C **11**, 1203 (1975).

[11]D. J. Ernst, Phys. Rev. C **19**, 896 (1979).

[12]R. M. DeVries and J. C. Peng, Phys. Rev. C **22**, 1055 (1980).
[13]H. Nishioka and R. C. Johnson, Phys. Rev. C **22**, 2457 (1980).
[14]D. M. Brink and G. R. Satchler, J. Phys. G **7**, 43 (1981).
[15]L. W. Townsend, J. W. Wilson, and H. B. Bidasaria, Can. J. Phys. **60**, 1514 (1982).
[16]N. J. DiGiacomo and R. M. DeVries, Comments Nucl. Part. Phys. **12**, 111 (1984).
[17]N. H. Kwong and J. Hüfner, Phys. Lett. **146B**, 370 (1984).
[18]M. Trefz, A. Faessler, and W. H. Dickhoff, Phys. Lett. **149B**, 459 (1984).
[19]A. Faessler, invited talk given at the HICOFED, Caen, 1986 [J. Phys. (Paris) Colloq. **47**, C4-111 (1986)].
[20]L. J. Cook, E. M. McMillan, J. M. Peterson, and D. C. Sewell, Phys. Rev. **7**, 75 (1949).
[21]B. D. Wilkins and G. Igo, Phys. Rev. **129**, 2198 (1963).
[22]J. J. H. Menet, E. E. Gross, J. J. Malanify, and A. Zucker, Phys. Rev. C **4**, 1114 (1971).
[23]P. U. Renberg, D. F. Meadsay, M. Pepin, P. Schwaller, B. Favier, and C. Richard-Serre, Nucl. Phys. **A183**, 81 (1972).
[24]D. L. Cheschire, R. W. Hugget, D. P. Johnson, W. V. Johnes, S. P. Rountree, S. D. Verma, W. K. H. Schmidt, R. J. Kurz, T. Bowen, and E. P. Krider, Phys. Rev. D **10**, 25 (1974).
[25]J. Jaros, A. Wagner, L. Anderson, O. Chamberlain, R. Z. Fuzesy, J. Gallup, W. Gorn, L. Schroeder, S. Shannon, G. Schapiro, and H. Stiner, Phys. Rev. C **18**, 2273 (1978).
[26]M. E. Brandan and A. Menchaca-Rocha, Phys. Rev. C **23**, 1272 (1981).
[27]A. Nadasen, P. Schwandt, P. P. Singh, W. W. Jacobs, A. D. Bacher, P. T. Debevec, M. D. Kaitchuck, and J. T. Meek, Phys. Rev. C **22**, 1023 (1981).
[28]A. J. Cole, W. D. Rae, M. E. Brandan, A. Dacal, B. G. Harvey, R. Legrain, M. J. Murphy, and R. G. Stokstad, Phys. Rev. Lett. **47**, 1705 (1981).
[29]M. Buenerd, J. Pinston, A. J. Cole, C. Guet, D. Lebrun, J. M. Loiseaux, P. Martin, E. Monnand, J. Mougey, H. Nifenecker, R. Ost, P. Perrin, C. Ristori, P. de Saintignon, F. Schussler, L. Carlen, H. A. Gustafsson, B. Jakobsson, T. Johansson, G. Jonsson, J. Krumlinde, I. Otterlund, H. Ryde, B. Schroder, G. Tibell, J. P. Bondorf, and O. B. Nielsen, Phys. Lett. **102B**, 242 (1981).
[30]H. G. Bohlen, M. R. Clover, G. Ingold, H. Lettau, and W. von Oertzen, Z. Phys. A **308**, 121 (1982).
[31]R. M. DeVries, N. J. DiGiacomo, J. S. Kapustinky, J. C. Peng, W. E. Sondheim, and J. W. Sunier, Phys. Rev. C **26**, 301 (1982).
[32]C. Perrin, S. Kox, N. Longequeue, J. B. Viano, M. Buenerd, R. Cherkaoui, A. J. Cole, A. Gamp, J. Menet, R. Ost, R. Bertholet, C. Guet, and J. Pinston, Phys. Rev. Lett. **49**, 1905 (1982).
[33]M. E. Brandan, J. Phys. G **9**, 197 (1983).
[34]S. Kox, A. Gamp, R. Cherkaoui, A. J. Cole, N. Longequeue, J. Menet, C. Perrin, and J. B. Viano, Nucl. Phys. **A420**, 162 (1984).
[35]M. Buenerd, A. Lounis, J. Chauvin, D. Lebrun, P. Martin, G. Duhamel, J. C. Gondrand, and P. de Saintignon, Nucl. Phys. **A424**, 313 (1984).
[36]N. Alamos, F. Auger, J. Barrette, B. Berthier, B. Fernandez, J. Gastebois, and L. Papineau, Phys. Lett. **137B**, 37 (1984).
[37]J. F. Bruandet, G. Costa, F. Glasser, C. Heitz, E. Liatard, Y. El-Masri, M. G. Saint Laurent, R. Seltz, R. de Swiniarski, and Tsan Ung Chan, GANIL Report No. 8, 1984 (unpublished).
[38]S. Kox, thèse d'état ISN 85-05, University of Grenoble, 1985 (unpublished).
[39]S. Kox, A. Gamp, C. Perrin, J. Arvieux, R. Bertholet, J. F. Bruandet, M. Buenerd, Y. El-Masri, N. Longequeue, and F. Merchez, Phys. Lett. **159B**, 15 (1985).
[40]J. F. Bruandet, invited talk given at the HICOFED, Caen, France, May, 1986 [J. Phys. (Paris) Colloq. **47**, C4-125 (1986)].
[41]T. D. Thomas, Phys. Rev. **116**, 703 (1959).
[42]J. R. Huizenga and G. Igo, Nucl. Phys. **29**, 462 (1962).
[43]L. C. Vaz and J. M. Alexander, Phys. Rev. C **10**, 464 (1974).
[44]J. R. Birkelund, J. R. Huizenga, H. Freiesleben, K. L. Wolf, J. P. Unid, and V. E. Viola, Jr., Phys. Rev. C **13**, 133 (1976).
[45]R. Bass, *Nuclear Reaction with Heavy-Ions, Texts and Monograms in Physics* (Springer-Verlag, Berlin, 1980).
[46]W. W. Wilke, J. R. Birkelund, H. J. Wollershein, A. D. Hoover, J. R. Huizenga, W. U. Shroder, and L. E. Tubbs, At. Data Nucl. Data Tables **5**, 25 (1980).
[47]S. K. Gupta and S. Kailas, Z. Phys. A **317**, 75 (1984).
[48]T. J. Gooding, Nucl. Phys. **12**, 241 (1959).
[49]J. B. Birks, *The Theory and Practice of Scintillation Counting* (Pergamon, Oxford, 1964).
[50]G. F. Knoll, *Radiation Detection and Measurements* (Wiley, New York, 1979), Sec. C.
[51]J. Chauvin, D. Lebrun, A. Lounis, and M. Buenerd, Phys. Rev. C **28**, 1970 (1983).
[52]J. Chauvin, D. Lebrun, F. Durand, and M. Buenerd, J. Phys. G **11**, 261 (1985).
[53]W. N. Hess, Rev. Mod. Phys. **30**, 368 (1958).
[54]R. Hofstadter, B. Hahn, A. W. Knudsen, and J. A. McIntyre, Phys. Rev. **95**, 512 (1954).
[55]C. W. De Jager, H. DeVries and C. DeVries, At. Data Nucl. Data Tables **14**, 479 (1974).
[56]A. S. Goldhaber, Phys. Lett. **53B**, 306 (1974).
[57]J. Mougey, R. Ost, M. Buenerd, A. J. Cole, C. Guet, D. Lebrun, J. M. Loiseaux, P. Martin, M. Maurel, E. Monnand, H. Nifenecker, P. Perrin, J. Pinston, R. Ristori, P. de Saintignon, F. Schussler, L. Carlen, B. Jakobsson, A. Oskarsson, I. Otterlund, B. Schroder, H. A. Gustafsson, T. Johansson, H. Ryde, J. P. Bondorf, O. B. Nielsen, and G. Tibell, Phys. Lett. **105B**, 25 (1981).
[58]B. G. Harvey, Nucl. Phys. **A444**, 498 (1985).
[59]A. J. Cole, Z. Phys. A **322**, 315 (1985).
[60]J. Y. Hostachy, private communication, and Nouvelles Saturne No. 11, 1986 (unpublished).
[61]H. Bohlen, H. Ossenbrick, H. Lettau, and W. von Oertzen, Z. Phys. A **320**, 237 (1985).
[62]J. Barrette, invited talk given at the HICOFED, Caen, France, May, 1986 [J. Phys. (Paris) Colloq. **47**, C4-141 (1986)].
[63]W. Treu, N. Frohlich, W. Galster, P. Duck, and H. Voit, Phys. Rev. C **22**, 2462 (1980).
[64]E. Clementi and C. Villi, Il Nuovo Cimento **2**, 176 (1955).
[65]N. J. DiGiacomo, R. M. DeVries, and J. C. Peng, Phys. Rev. Lett. **45**, 527 (1980).
[66]N. J. DiGiacomo, J. C. Peng, and R. M. DeVries, Phys. Lett. **101B**, 383 (1981).
[67]W. D. Myers, Nucl. Phys. **A204**, 465 (1973).